

# Three-body losses of a polarized Fermi gas near a $p$ -wave Feshbach resonance in effective field theory

M. Schmidt,<sup>1</sup> L. Platter,<sup>2,3</sup> and H.-W. Hammer<sup>1,4</sup>

<sup>1</sup>*Institut für Kernphysik, Technische Universität Darmstadt, 64289 Darmstadt, Germany*

<sup>2</sup>*Department of Physics and Astronomy,*

*University of Tennessee, Knoxville, TN 37996, USA*

<sup>3</sup>*Physics Division, Oak Ridge National Laboratory, Oak Ridge, TN 37831, USA*

<sup>4</sup>*ExtreMe Matter Institute EMMI, GSI Helmholtzzentrum für  
Schwerionenforschung GmbH, 64291 Darmstadt, Germany*

(Dated: November 15, 2019)

## Abstract

We study three-body recombination of fully spin-polarized  ${}^6\text{Li}$  atoms that are interacting resonantly in relative  $p$ -waves. Motivated by a recent experiment, we focus on negative scattering volumes where three atoms recombine into a deep dimer and another atom. We calculate the three-body recombination rate using a Faddeev equation derived from effective field theory. In particular, we study the magnetic field and temperature dependences of the loss rate and use the recombination data to determine the effective range of the  $p$ -wave atom-atom interaction. We also predict the existence of a shallow three-body bound state that manifests itself as a prominent feature in the energy-dependent three-body recombination rate.

## I. INTRODUCTION

Experiments with ultracold atomic gases provide a unique way to explore the interactions between atoms. Specifically, strongly interacting systems have recently received a lot of attention [1–5]. For example, the loss rate of an ultracold gas of strongly interacting bosons will display discrete scale invariance when it is measured as a function of the scattering length. This discrete scale invariance is related to the well-known Efimov effect [6] and leads to a log-periodic dependence of the three-body loss rate on the scattering length [7–10]. Three-body losses occur in ultracold atomic gases as a result of three-body collisions in which the atoms gain kinetic energy due to the formation of a two-body bound state. Indeed, the Efimov effect was first observed through its signature in three-body losses in a cold gas of Cs atoms [11].

Identical fermions cannot interact in a relative  $s$ -wave due to the Pauli principle. However, their  $p$ -wave scattering volume can be tuned and a number of experiments have examined the features of strongly interacting Fermi gases [12–17]. The Efimov effect does not occur in these systems [18–20], however, losses still occur through recombination processes into shallow or deep dimers. The three-body losses in spin-polarized ultracold gases of  ${}^6\text{Li}$  have recently been studied in the group of Takashi Mukaiyama at Osaka University focusing on scaling laws [15], unitary-limited behavior [16], and the role of cascade processes [17].

In this paper, we focus on the data taken by Waseem *et al.* in [16]. Specifically, they considered the  $|F = 1/2, m_F = +1/2\rangle$  hyperfine state and measured the loss rate at large negative  $p$ -wave scattering volume, enhanced by a Feshbach resonance at  $B_0 = 159.17(5)$  G. At negative scattering volume, three atoms recombine into a so-called deep dimer, *i.e.*, a dimer whose binding energy is so large that it cannot be described by the parameters of the effective range expansion. The authors of this work used a simplified Breit-Wigner model for the energy-dependent three-body recombination rate coefficient  $K_3(E)$  to determine information about the atom-atom interaction and to model the temperature-dependent three-body loss coefficient  $L_3(T)$ . While they managed to reproduce the measured loss data appropriately, we will discuss in detail that their simplified approach has also some important limitations.

It is particularly important to have an accurate microscopic description for the three-body recombination if the goal is to extract two-body observables from three-body processes with some understanding of the resulting uncertainties. Various approaches can be used to develop a microscopic description of this process. Effective field theory (EFT) uses the separation between short- and long-range scales in a system to construct a controlled expansion. It has been applied successfully in particle, nuclear and atomic physics [1, 21, 22]. The parameters that appear in the EFT description of atomic systems with strong interactions can be related directly to the effective range parameters. This approach is therefore model independent and facilitates an unbiased analysis of experimental data. Systems with  $p$ -wave interactions have been studied using the short-range effective field theory previously [20]. It was found that a real three-body parameter is required for renormalization. However, the emphasis of this work was on renormalization issues and the spectrum of three-body states.

Here, we will use EFT to study the three-body loss rate into deep dimers at finite temperature with the parameters relevant to the experimental measurements by Waseem *et al.* [16]. We will construct the interaction of two atoms in a relative  $p$ -wave and use it to derive an integral equation whose solution allows us to compute the three-body recombination rate  $K_3(E)$ . Temperature averaging then yields the three-body loss coefficient  $L_3(T)$ . Compari-

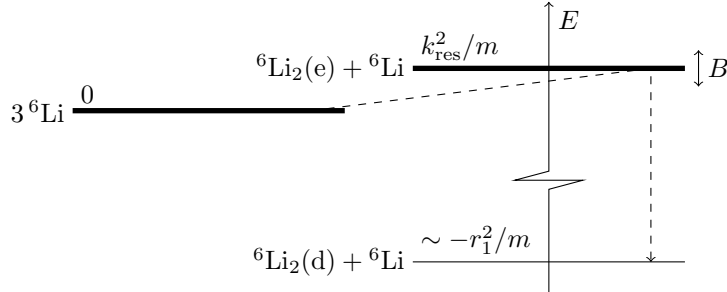


Figure 1: Level scheme of three spin-polarized  ${}^6\text{Li}$  atoms in the hyperfine state  $|F = 1/2, m_F = +1/2\rangle$ . Three-body recombination into a deeply bound state  ${}^6\text{Li}_2(\text{d})$  proceeds through the Feshbach resonance state  ${}^6\text{Li}_2(\text{e})$ . Its position  $k_{\text{res}}^2(B)/m$  can be tuned by a magnetic field  $B$ .

son with the data obtained by Waseem *et al.* will let us draw conclusions about the features of the two-body interaction such as the  $p$ -wave effective range. Moreover, it will allow us to tie these features to other three-body observables such as the energy of a shallow three-body bound state.

This manuscript is organized as follows. In Secs. II and III, we will introduce our microscopic framework to calculate the three-body loss coefficient. Some details of the EFT framework are given in the Appendices. Our results are presented and compared to the data by Waseem *et al.* [16] in Sec. IV. We end with a short summary and outlook in Sec. V.

## II. RECOMBINATION NEAR A $p$ -WAVE RESONANCE

At sufficiently low energies, the elastic scattering properties of particles can be quantified using the effective range expansion. In the  $p$ -wave, the expansion is

$$k^3 \cot \delta_1 = -\frac{1}{a_1} + \frac{r_1}{2} k^2 + \dots, \quad (1)$$

where  $\delta_1$  is the scattering phase shift,  $a_1$  denotes the scattering volume,  $r_1$  is the effective range, and the ellipses denote higher order terms. We note that our definition of the effective range  $r_1$  differs by a factor of  $-2$  from the definition used in Ref. [16].

The level scheme of three spin-polarized  ${}^6\text{Li}$  atoms in the hyperfine state  $|F = 1/2, m_F = +1/2\rangle$  is illustrated in Fig. 1. Two identical  ${}^6\text{Li}$  atoms form a deeply bound state denoted  ${}^6\text{Li}_2(\text{d})$ . The Feshbach resonance creates an excited state  ${}^6\text{Li}_2(\text{e})$ , whose position can be tuned by changing the magnetic field  $B$ . The scattering volume of two  ${}^6\text{Li}$  atoms in the  $|F = 1/2, m_F = +1/2\rangle$  state,  $a_1$ , diverges at the resonance position,  $B_0 = 159.17(5)$  G. For  $B \approx B_0$ , the magnetic field dependence has the form

$$a_1(B) = a_{1,\text{bg}} \left( 1 + \frac{\Delta B}{B - B_0} \right) \approx \frac{a_{1,\text{bg}} \Delta B}{B - B_0}, \quad (2)$$

where  $a_{1,\text{bg}} < 0$  is the background scattering volume and  $\Delta B > 0$  is the resonance width [16].<sup>1</sup> As input, we use the value  $a_{1,\text{bg}} \Delta B = -2.8(3) \times 10^6 a_{\text{B}}^3$  G, obtained in a fit to the

<sup>1</sup> For detunings  $B - B_0 < 0.5$  G as in [16], the constant term in Eq. (2) is less than 1% of the total and can be neglected.

thermalization rate of the spin-polarized  ${}^6\text{Li}$  gas by Nakasuji *et al.* [23]. For fixed  $B \approx B_0$ ,  $a_1(B)$  is then given with an uncertainty of roughly 30%.

The  $p$ -wave effective range  $r_1$  is usually assumed to depend weakly on  $B$  in the immediate vicinity of  $B_0$  [16, 23, 24]. Waseem *et al.* suggested the near-resonance estimate

$$(r_1)_{\text{est}} \equiv \frac{2}{m \delta\mu a_{1,\text{bg}} \Delta B} = -0.182(20) a_{\text{B}}^{-1}, \quad (3)$$

and used it in their analysis of the experimental data [16]. In Eq. (3),  $\delta\mu = 113(7) k_{\text{B}} \mu\text{K G}^{-1}$  denotes the relative magnetic moment between  ${}^6\text{Li}_2(\text{e})$  and two  ${}^6\text{Li}$  atoms with  $k_{\text{B}}$  being Boltzmann’s constant. We adopt the assumption that  $r_1$  is constant in  $B$ . However, we note that different estimates for  $r_1$  have been given that differ significantly from  $(r_1)_{\text{est}}$ . First, Bruun *et al.* derived Eq. (3) only for two bosons near an  $s$ -wave Feshbach resonance [25]. Second, Nakasuji *et al.* obtained a different value  $-0.116(10) a_{\text{B}}^{-1}$  in their fit to the thermalization rate [23]. They also cited an even smaller theory prediction  $-0.096(6) a_{\text{B}}^{-1}$  by Julienne (Ref. [29] of their work). This value deviates by roughly 50% from Eq. (3). Thus,  $r_1$  introduces the largest uncertainty to the study. It is one goal of this work to predict  $r_1$  from data of the three-body loss coefficient  $L_3$ .

In the experiment by Waseem *et al.*, recombination was studied for  $B - B_0 > 0$  ( $a_1 < 0$ ), where the process can be distinguished from background losses [16]. Thus, we restrict ourselves to this region when calculating  $L_3$ . On this side of the Feshbach resonance, the two-body system has a resonance pole above threshold representing the  ${}^6\text{Li}_2(\text{e})$  state.<sup>2</sup> The position of the corresponding maximum of the scattering amplitude on the real  $k$  axis will be denoted by  $k_{\text{res}}$  (cf. Fig. 1). It varies with  $B$  and will be denoted “resonance momentum” in the following. For large scattering volume, the resonance momentum can be approximated by [26, 27]

$$k_{\text{res}}(B) = \sqrt{\frac{2}{a_1(B)r_1}}. \quad (4)$$

Note that the Feshbach resonance introduces a strong separation of momentum scales to the two-body system. In particular, the resonance momentum  $k_{\text{res}}(B)$  is much smaller than the natural (high) momentum scale set by the effective range  $r_1$ . Such a separation is an important requirement for the EFT approach. In the system at hand, it enables an expansion of the two-body scattering amplitude in terms of the ratio  $\chi_2(B) \equiv k_{\text{res}}(B)/r_1 \ll 1$ . This expansion yields a simple Breit-Wigner-like diatom propagator at leading order in the expansion in  $\chi_2(B)$  [27]. In the following, we restrict our analysis to leading order (LO) in the expansion in  $\chi_2(B)$ .

For  $B - B_0 > 0$ , three-body recombination proceeds in the absence of a shallow dimer state only into deep dimer states  ${}^6\text{Li}_2(\text{d}) + {}^6\text{Li}$ . Such a process involves a large excess of kinetic energy  $\sim r_1^2/m$  outside our EFT’s applicability region, *i.e.*, the recombination process happens when all three atoms are very close together. While the process cannot be described in detail in the framework of our EFT, the total rate for recombination into deep dimers can be described by making the three-body parameter complex [28]. This corresponds to using an optical three-body potential to model the losses at short distances which can be treated in perturbation theory [10].

<sup>2</sup> For  $B - B_0 < 0$  (corresponding to  $a_1 > 0$ ),  ${}^6\text{Li}_2(\text{e})$  is a shallow bound state.

As shown by Esry *et al.*, the recombination rate of three identical fermions vanishes at total kinetic energy  $E = 0$  [29]. More specifically, it obeys the threshold law  $K_3 \propto E^2$  in the partial wave channel  $J^P = 1^+$  and is suppressed by further powers of  $E$  for other  $J^P$ . Thus, we focus on the  $1^+$  channel at LO. To calculate the recombination rate  $K_3(p_E)$ , the absolute square of the matrix element for the recombination process in the  $J^P = 1^+$  channel,  $\mathcal{M}^{1m_J}$  ( $m_J \in \{-1, 0, 1\}$ ), has to be integrated over incoming momenta  $\mathbf{p}_1, \mathbf{p}_2, \mathbf{p}_3$ , summed over  $m'_J$  and divided by the three-body phase space  $\phi_3(p_E)$ , *i.e.*,

$$K_3(p_E) = \frac{1}{\phi_3(p_E)} \left( \prod_{i=1}^3 \int \frac{d^3 p_i}{(2\pi)^3} \right) (2\pi)^4 \delta^{(3)} \left( \sum_{i=1}^3 \mathbf{p}_i \right) \delta \left( \frac{p_E^2}{m} - \sum_{i=1}^3 \frac{p_i^2}{2m} \right) \times \sum_{m'_J} |i\mathcal{M}^{1m_J}(\{\mathbf{p}_i\}; p_E)|^2, \quad (5)$$

where  $p_E^2/m \equiv E$ . This expression can partially be evaluated analytically by integrating over the  $\delta$ -functions as will be discussed below.

Data for three-body recombination is only available at finite temperature  $T \sim \mu\text{K}$  [16]. For this reason, we have to calculate the thermal average of  $K_3$ . The energy  $E$  is distributed according to the Boltzmann distribution of three equal-mass particles which is proportional to  $E^2 \exp[-E/(k_B T)]$ ; see, *e.g.*, Refs. [30, 31]. In terms of  $p_E$ , it follows that

$$\langle K_3 \rangle (T) = \frac{1}{(m k_B T)^3} \int_0^\infty dp_E p_E^5 e^{-p_E^2/(m k_B T)} K_3(p_E). \quad (6)$$

The thermal average is directly proportional to the experimentally measured loss coefficient [8, 16]

$$L_3(T) = \frac{3}{6} \langle K_3 \rangle (T). \quad (7)$$

We reiterate that our focus is on three-body recombination into deep dimers. However, the same formalism can be used to study recombination into shallow dimers, *i.e.*, three-body recombination for positive two-body scattering volume  $a_1$ . A preliminary study of this case can be found in Ref. [27].

### III. THREE-BODY RECOMBINATION MATRIX ELEMENT

In order to calculate the matrix element  $\mathcal{M}^{1m_J}$  in Eq. (5), we require the atom-diatom scattering amplitude  $T^{(1^+)}$  in off-shell kinematics. This amplitude can be obtained by solving an integral equation derived from effective field theory. In general, the total angular momentum  $\mathbf{J} = \mathbf{l} + \mathbf{L}$  is the sum of the atom-atom orbital angular momentum  $\mathbf{l}$  ( $l = 1$ ) and the diatom-atom orbital angular momentum  $\mathbf{L}$ , implying  $P = (-1)^{1+L}$ . Thus, at small energies, the leading partial wave channel  $J^P = 1^+$  is given by the single combination  $l = L = J = 1$ . We restrict ourselves to this channel at LO. The theoretical uncertainty introduced by this approximation will be addressed at the end of this chapter. The partial-wave projected integral equation for the amplitude  $T^{(1^+)}$  reads [27]

$$T^{(1^+)}(p, p'; p_E) = -V^{(1^+)}(p, p'; p_E) + \int_0^\Lambda \frac{dq q^2}{2\pi^2} V^{(1^+)}(p, q; p_E) G_\pi(\tilde{k}(q^2)) T^{(1^+)}(q, p'; p_E), \quad (8)$$

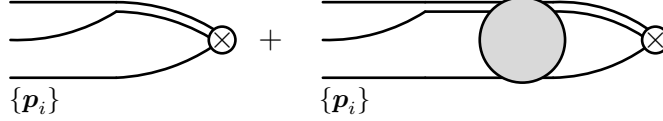


Figure 2: Matrix element for three-body recombination into a deeply bound state. The cross indicates the pointlike vertex for recombination into the deep dimer. The gray blob denotes the atom-diatom amplitude  $T^{(1+)}$  which is the solution of Eq. (8).

where

$$\tilde{k}(q^2) = i\sqrt{-p_E^2 + \frac{3}{4}q^2 - i\epsilon}, \quad (9)$$

is a momentum variable and  $G_\pi$  is the Breit-Wigner-like LO diatom propagator

$$iG_\pi(\tilde{k}) = i \left[ -a_1^{-1}(B) + \frac{r_1}{2}\tilde{k}^2 - ik_{\text{res}}^3(B)\theta(B - B_0) \right]^{-1}, \quad (10)$$

which contains information on the two-body effective range parameters. Moreover,  $p$  ( $p'$ ) denotes the incoming (outgoing) atom-diatom relative momentum and  $p_E \equiv i(-mE - i\epsilon)^{1/2}$  is the momentum scale set by the total kinetic energy. The quantity

$$V^{(1+)}(p, q; p_E) = 8\pi [Q_0 - Q_2] \left( \frac{p_E^2 - p^2 - q^2}{pq} \right) + \frac{H^{(1+)}(\Lambda)pq}{\Lambda^2} \quad (11)$$

is the exchange potential arising from partial wave projection of the single-atom exchange contribution where  $Q_0$  and  $Q_2$  are Legendre functions of the second kind in the convention of Ref. [32]. The integral equation (8) is equipped with a momentum cutoff of natural order,  $\Lambda \sim r_1$  or larger, which also appears in the three-body force term. The three-body force  $H^{(1+)}(\Lambda)$  is required for renormalization of the atom-dimer amplitude [20] and depends on the cutoff  $\Lambda$ . Details of the derivation including the Feynman rules and partial wave projection can be found in Appendices A and B. Note that for  $B > B_0$ , the diatom is unstable and does not represent an asymptotic state. However, the quantity  $T^{(1+)}(p, p'; p_E)$  is required in off-shell kinematics to calculate the three-body recombination matrix element  $\mathcal{M}^{1m_J}$ .

The three-body recombination matrix element  $\mathcal{M}^{1m_J}$ , depicted in Fig. 2, depends on the three incoming atom momenta  $\mathbf{p}_i$  ( $i \in \{1, 2, 3\}$ ). For identical fermions, the matrix element must be antisymmetric under exchange of each pair of momenta  $\mathbf{p}_i, \mathbf{p}_j$  ( $i \neq j$ ). This property is automatically taken care of by the anticommutation relations of the atom field operators  $\psi, \psi^\dagger$  introduced in Appendix A. Applying the Feynman rules dictated by the effective Lagrangian of Eq. (A2) in the Appendix to the two diagrams in Fig. 2, we find

$$i\mathcal{M}^{1m_J}(\{\mathbf{p}_i\}; p_E) = iF^{(1+)}(\Lambda) 3\sqrt{\frac{2\pi}{m}} \sum_{\pi \in \mathcal{C}_3} \{\mathbf{p}_{\pi(1)} - \mathbf{p}_{\pi(2)}\}_{1m_i} G_\pi(\tilde{k}(p_{\pi(3)}^2)) \\ \times \left( C_{1m_L, 1m_i}^{1m_J} \{\mathbf{p}_{\pi(3)}\}_{1m_L} - \int \frac{d^3q}{(2\pi)^3} T^{m_i, m'_i}(\mathbf{p}_{\pi(3)}, \mathbf{q}; p_E) G_\pi(\tilde{k}(q^2)) C_{1m_L, 1m'_i}^{1m_J} \{\mathbf{q}\}_{1m_L} \right), \quad (12)$$

where  $C_{Lm_L, lm'_l}^{Jm_J}$  is a Clebsch-Gordan coefficient that couples the angular momenta  $\mathbf{l}$  and  $\mathbf{L}$  to  $\mathbf{J}$  and the sum is over all even permutations  $\pi$  of (123), denoted  $\mathcal{C}_3$ . Sums over  $m_i, m'_i$ , and  $m_L$  are implicit. The coefficient of the pointlike vertex for recombination into

the deep  $p$ -wave dimer is given by  $F^{(1^+)}(\Lambda)$ . This regulator-dependent constant acts as a short-range optical potential. The general equation for  $T^{m_l, m'_l}$  including all partial waves is given in Appendix B. At LO, the unprojected amplitude  $T^{m_l, m'_l}$  in Eq. (12) reduces to its  $1^+$  component, *i.e.*,

$$T^{m_l, m'_l}(\mathbf{p}, \mathbf{q}; p_E) = T^{(1^+)}(p, q; p_E) 4\pi \sum_{m_J} (\mathbf{Y}_{(1,1)1m_J}(\hat{\mathbf{p}}))^{m_l} (\mathbf{Y}_{(1,1)1m_J}(\hat{\mathbf{q}}))^{m'_l} \quad (13)$$

in the convention of Eq. (B2b). The tensor structure  $\{\cdot\}_{1m}$  in Eq. (12) is defined in Eq. (A3).

To evaluate the expression for the recombination rate in Eq. (5), we further need the three-body phase space

$$\phi_3(p_E) = \frac{m p_E^4}{24\sqrt{3}\pi^2}. \quad (14)$$

Inserting Eq. (12) and integrating over the  $\delta$ -functions, we obtain

$$K_3(p_E) = \frac{|F^{(1^+)}(\Lambda)|^2}{m} \frac{432\sqrt{3}}{p_E^4} \int_0^{\frac{2}{\sqrt{3}}p_E} dp_A p_A \int_0^{\frac{2}{\sqrt{3}}p_E} dp_B p_B \theta(1 - |x_0|) \times \left[ |p_A J(p_B; p_E)|^2 + 2 \operatorname{Re} \left( p_B J(p_A; p_E) [p_A J(p_B; p_E)]^* \right) \right], \quad (15)$$

where

$$x_0 \equiv \frac{1}{p_A p_B} (p_E^2 - p_A^2 - p_B^2), \quad (16a)$$

$$J(p; p_E) \equiv G_\pi \left( \tilde{k}(p^2) \right) \left( p - \int_0^\Lambda \frac{dq q^2}{2\pi^2} T^{(1^+)}(p, q; p_E) G_\pi \left( \tilde{k}(q^2) \right) q \right). \quad (16b)$$

The integral contained in the definition in  $J$  diverges as  $\Lambda \rightarrow \infty$ . This cutoff dependence is absorbed by an appropriate running of the short-range factor  $|F^{(1^+)}(\Lambda)|^2$  with  $\Lambda$ . The running of  $F^{(1^+)}$  can be obtained by making the three-body force  $H^{(1^+)}$  in Eq. (11) required to renormalize  $T^{(1^+)}$  complex. Thus, the running of  $F^{(1^+)}$  with the cutoff  $\Lambda$  is fully determined by the running of  $H^{(1^+)}$ . A similar procedure was previously used to describe three-body recombination into deep  $s$ -wave dimers [10].

Before we go on, we expand on the expected size of omitted partial waves as compared to  $J^P = 1^+$ . For sufficiently small energies, their contributions to the recombination rate involve at least one more factor  $E$  [29]. Naively, one would compare this factor to the breakdown scale  $r_1^2/m$  set by the  $p$ -wave effective range. For  $p_E \lesssim k_{\text{res}}(B) = \chi_2(B)r_1$ , that would yield an *a priori* uncertainty  $p_E^2/r_1^2 \lesssim \chi_2^2(B)$  which is very small ( $\lesssim 0.01\%$  for  $B - B_0 \leq 0.5$  G). In obtaining this estimate, we have used the threshold laws of Ref. [29]. The work of Suno *et al.*, however, suggests that the threshold laws fail at  $p_E = k_{\text{res}}(B)$  [33]. At this point, formerly subleading channels may become comparable to  $J^P = 1^+$ . As a consequence, we apply our LO framework only to the low-energy region  $p_E < k_{\text{res}}(B)$ . The *a priori* LO uncertainty at fixed energy can then be written as  $\chi_3(B, E) \equiv p_E^2/k_{\text{res}}^2(B) < 1$ .

To estimate the LO uncertainty  $\tilde{\chi}_3(B, T)$  at finite temperature, we set  $p_E$  to the maximum of the Boltzmann weighting factor in Eq. (6), *i.e.*, to

$$p_T \equiv \sqrt{\frac{5}{2} m k_B T}. \quad (17)$$

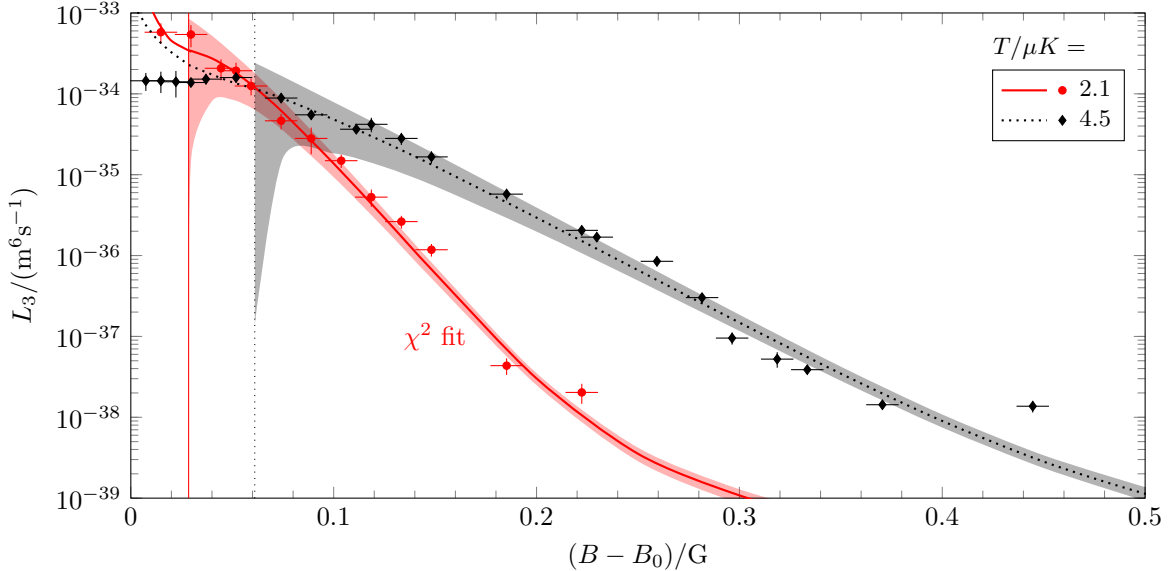


Figure 3: Loss coefficient  $L_3$  as function of the field detuning  $B - B_0$  for two temperatures  $T$  at  $\Lambda = 0.4 a_B^{-1}$ . Vertical gridlines mark points at which  $k_{\text{res}}(B) = p_T$ . They separate the respective unitary (left) from the nonunitary (right) regime. The solid red curve is a  $\chi^2$  fit in  $(r_1, H^{(1+)}, F^{(1+)})$  to the  $T = 2.1 \mu\text{K}$  data in the nonunitary regime for  $a_{1,\text{bg}} \Delta B = -2.8 \times 10^6 a_B^3 \text{ G}$ . The black dotted curve is the resulting prediction for  $T = 4.5 \mu\text{K}$ . Uncertainty bands in the nonunitary regime follow from NLO corrections of order  $p_T^2/k_{\text{res}}^2(B) < 1$  and from the experimental uncertainty of  $a_{1,\text{bg}} \Delta B$ . Naive application of the theory to the unitary regime leads to an overestimation of the data.

This yields the expression

$$\tilde{\chi}_3(B, T) \equiv p_T^2/k_{\text{res}}^2(B) \approx \frac{r_1}{2} a_{1,\text{bg}} \Delta B \frac{5}{2} m k_B \frac{T}{B - B_0}, \quad (18)$$

where Eqs. (2) and (4) have been used. Note that we aim to determine  $r_1$  from the data and thus do not use the approximate relation (3).

## IV. RESULTS

### A. Fit of free parameters and comparison with experiment

The data obtained in Ref. [16] can be divided into two different regimes, the unitary regime and the non-unitary regime. We define the unitary regime as the temperature domain in which the resonance momentum  $k_{\text{res}}$  is smaller than the thermal momentum scale  $p_T$  defined in Eq. (17). For a given resonance momentum  $k_{\text{res}}$ , the unitary regime sets in at temperatures larger than

$$T_{\text{unitary}} > \frac{2k_{\text{res}}^2}{5mk_B}. \quad (19)$$

We do not expect our EFT to work in this regime since the expansion parameter  $\tilde{\chi}_3(B, T) \gtrsim 1$ . For convenience, we will also drop the superscript 1+ in the three-body terms  $H$  and  $F$  from now on.



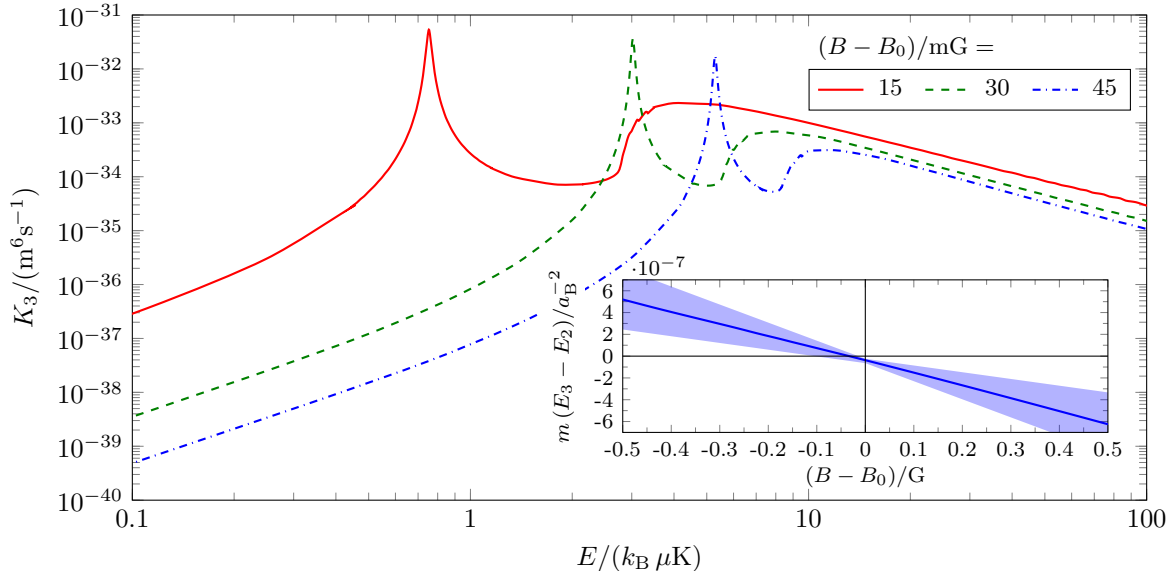


Figure 4: Recombination rate coefficient  $K_3$  as function of the energy  $E$  for several field detunings  $B - B_0$  at  $\Lambda = 0.4 a_B^{-1}$ . The inset shows the rescaled energy gap  $m(E_3 - E_2)$  as a function  $B - B_0 = 0$  with an error estimate given by the shaded band.

We use our approach to fit the effective range  $r_1$ , the three-body force  $H$ , and the short-distance three-body parameter  $F$  to the experimental data for  $T = 2.1 \mu\text{K}$  from Ref. [16]. Our results are renormalization group invariant and independent of  $\Lambda$ , but for definiteness we use an ultraviolet cutoff  $\Lambda = 0.4 a_B^{-1}$  in the integral equations. We find an effective range  $r_1 = -0.11(2) a_B^{-1}$  which is of the same order of magnitude as the result by Waseem *et al.* but deviates by 60 %. For the three-body force, we find  $H = 4_{-7}^{+5}$  and for the short-distance three-body parameter we obtain  $\log_{10}(F/m^2) = 49.8_{-0.1}^{+0.2}$ . We emphasize that these two quantities are not observables and depend on the ultraviolet cutoff  $\Lambda$  used to solve Eq. (8).

The red solid line in Fig. 3 shows the fitted loss coefficient  $L_3$  in comparison to the experimental data (red circles). Experimental data in the unitary regime was excluded in the fit. These data points are to the left of the red solid line in that figure. Once the parameters of our approach are determined, we can use Eqs. (6) and (7) to predict the loss rate at a different temperature. Figure 3 shows also the resulting prediction for the loss rate at a temperature  $4.5 \mu\text{K}$  (black dotted line) in comparison to the experimental data from Ref. [16] (black diamonds). Our results describe data at these small temperatures relatively well.

The finite-temperature averaging of the energy-dependent recombination rate coefficient  $K_3$  smears out the resonance features from the three-body loss rate. In Fig. 4, we show  $K_3$  as a function of the energy for different magnetic field detunings. The curves have been generated with the parameters obtained in the fit to the  $T = 2.1 \mu\text{K}$  data from Ref. [16] discussed above. They display a strong peak at lower energies followed by a sudden increase and a smooth fall off. The peak on the left is caused by the existence of a three-body resonance below the two-body resonance. Its position is controlled by the three-body force  $H$ . The sudden rise in  $K_3$  to the right of the peak is the signature of the two-body resonance.

Given the fit results for  $r_1$  and  $H$ , the difference of the three- and two-body resonance energies,  $E_3 - E_2$ , is a function of the scattering volume, *i.e.*, the magnetic field detuning,

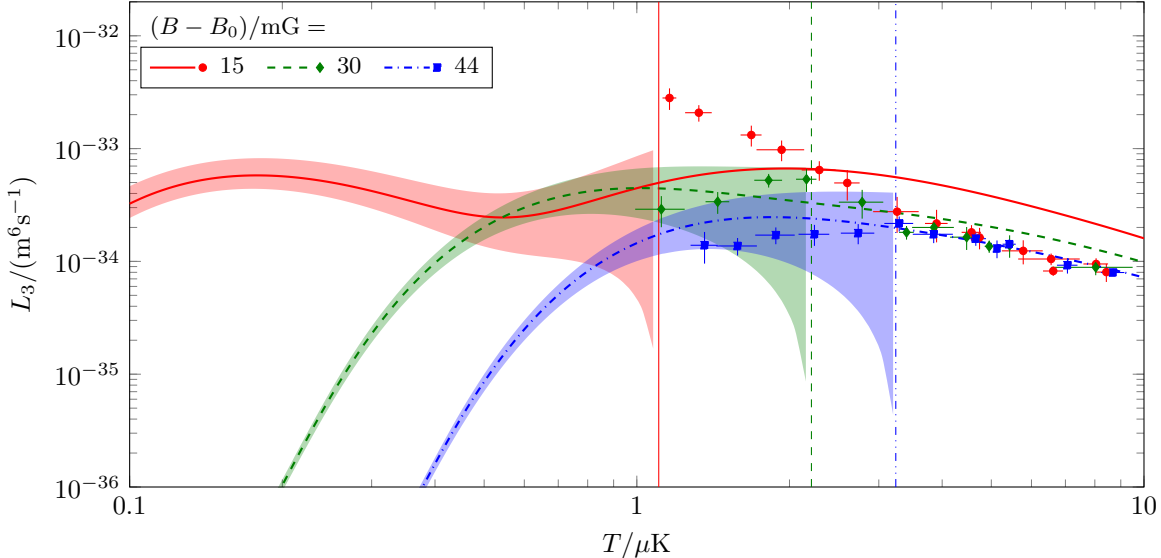


Figure 5: Loss coefficient  $L_3$  as function of the temperature  $T$  for several field detunings  $B - B_0$  at  $\Lambda = 0.4 a_B^{-1}$  ( $\chi^2$ -fit predictions). Vertical gridlines at  $k_T = k_{\text{res}}$  separate the nonunitary (left) from the unitary (right) regime. Uncertainty bands are obtained as in Fig. 3. For clarity, they are omitted for the higher detunings.

only. Thus, our approach allows us to predict the magnetic field dependence of the three-body resonance energy  $E_3$ . In the inset of Fig. 4, we show the rescaled energy gap  $m(E_3 - E_2)$  as a blue line. For  $B - B_0 > 0$ , the three-body resonance is below the two-body resonance and  $E_3 - E_2$  is negative. Near  $B - B_0 = 0$ ,  $E_3$  is linear in  $B$  just like  $E_2$  and the three-body resonance crosses the two-body energy. In the region  $B - B_0 < 0$ , the two-body resonance turns into a shallow bound state and the energy difference  $E_3 - E_2$  becomes positive.

Note that corrections to our prediction should arise from omitted  $J^P$  channels. Contributions of these channels to the loss rate coefficient  $L_3(B)$  in the fit regime should have relative sizes  $0 \leq \chi_3(B, T) \leq 1$ ; see Eq. (18). Gaussian uncertainty propagation then implies a relative uncertainty of 46% for the  $\chi^2$  value of our fit. This number can be used as an estimate for the uncertainties of the offset  $\alpha$  and slope  $\beta$  of the  $m(E_3 - E_2) = \alpha + \beta(B - B_0)$  curve. We obtain  $\alpha = -0.4(2) \times 10^{-7} a_B^{-2}$  and  $\beta = -11(5) \times 10^{-7} a_B^{-2}/G$  which yields the blue band depicted in the inset of Fig. 4.

Finally, Fig. 5 shows the temperature averaged loss rate  $L_3$  as a function of the temperature  $T$  for different detunings  $B - B_0$ . The vertical lines denote the beginning of the unitary regime as given by Eq. (19). While they reproduce the expected  $T^{-2}$  behavior at large temperatures, the curves are not independent of  $B$  in the unitary regime. Instead, they are separated by factors of 1.3-1.5. We expect that effects from the unitary cut will be important in this region where the system is able to probe the resonance peak [26]. Moreover, the contribution from spin-parity channels different from  $J^P = 1^+$  could be important. Even though suppressed close to  $E = 0$ , they might contribute significantly at finite temperature. It would also be instructive to iterate effects of the short-range three-body factor  $F$ . A nonperturbative treatment would presumably change the behavior at larger energies. Understanding the loss rate in this region is left to future work.

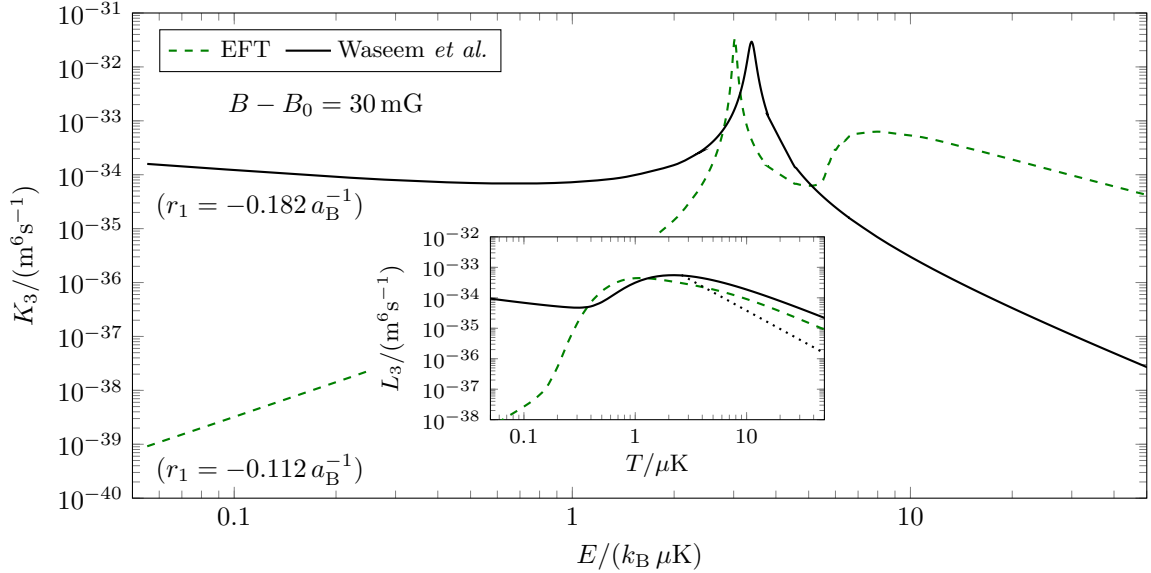


Figure 6: Comparison of the energy-dependent recombination rate coefficient  $K_3$  from our EFT calculation (dashed curve) and from the model by Waseem *et al.* [16] (solid curve) as function of the energy  $E$  for a magnetic field detuning of  $B - B_0 = 30$  mG. The inset shows the same comparison for the temperature-dependent loss coefficient  $L_3$  where the dotted curve shows the  $E^{-2}$  behavior expected from unitarity. The dramatically different behavior of the recombination rates at low energies leads to different predictions for the loss rates at temperatures below  $0.5 \mu\text{K}$  only.

## B. Comparison with Waseem *et al.*

We now compare our results to the two-body model employed by Waseem *et al.* [16],

$$K_3^{\text{Waseem}}(E) = \frac{144\sqrt{3}\pi^2}{m^3 E^2} \frac{\Gamma_e \Gamma_d}{(E - E_b)^2 + (\Gamma_e + \Gamma_d)^4/4}, \quad (20)$$

where  $\Gamma_e = -4\sqrt{m}E^{3/2}/r_1$ ,  $\Gamma_d = -4/(mr_1 a_1)$ , and  $E_b = k_{\text{res}}^2/m$  is the real part of the resonance energy.<sup>3</sup> While the temperature averaged loss coefficient  $L_3$  looks very similar to our result, the energy-dependent recombination rate coefficient  $K_3$  behaves very differently.

This can be seen in Fig. 6, where we compare the three-body recombination model in Eq. (20) and our results for a magnetic field detuning of  $B - B_0 = 15$  mG. While the temperature-averaged loss coefficient  $L_3$  shown in the inset for both approaches agrees for temperatures  $T > 1 \mu\text{K}$  measured in the experiment by Waseem *et al.*, the energy-dependent rate coefficient  $K_3$  shows stark differences. The rate calculated in the EFT approach falls off at small energies as  $E^2$  while the model in Eq. (20) grows as  $E^{-1/2}$ . Both approaches show a peak around  $E = 3 k_B \mu\text{K}$  but the microscopic origin is very different. In the model of Waseem *et al.* it is simply associated with the Breit-Wigner form put in by hand, while the resonance in the full three-body treatment in the EFT framework is dynamically generated by the  $p$ -wave atom-atom interactions. Finally, there is a shoulder around  $E = 7 k_B \mu\text{K}$  in the EFT framework which is not present in the model.

<sup>3</sup> Note that we have converted Eq. (20) to our conventions where  $\hbar = 1$ .

Currently, the data for the temperature averaged loss rate is not able to distinguish between the two approaches and thus the underlying microphysics. The inset of Fig. 6, however, suggests that a new measurement at lower temperatures  $T \leq 0.5 \mu\text{K}$  should be able to distinguish between the two scenarios.

## V. SUMMARY

In this work, we have considered the temperature dependent three-body loss rate for a gas of identical fermions with resonant  $p$ -wave interactions. We have used an effective field theory approach to derive integral equations that describe the scattering of three fermions and used them to evaluate the rate for three-body recombination into deeply bound dimers and another atom. Our approach requires the determination of four parameters to become predictive; the scattering volume  $a_1$ , the effective range  $r_1$ , and two pieces of three-body information to determine the short-range three-body parameters  $H$  and  $F$ . The latter acts as an optical potential and parameterizes the coupling of the three-body system to final state channels with deep dimers. We have used the known magnetic field dependence of the scattering volume  $a_1$  and the experimental data from Waseem *et al.* [16], to fit the remaining parameters  $r_1$ ,  $H$ , and  $F$ . Once these parameters are determined, we were also able to determine the position and magnetic field dependence of a fermionic three-body state with  $J^P = 1^+$ . We note that this three-body resonance could lead to interesting features in the three-body recombination rate on the positive scattering volume side of the Feshbach resonance, where the three-body state is a resonance close to the atom-dimer threshold. For positive scattering volume, it would also be interesting to consider atom-dimer relaxation as an additional benchmark to our approach.

While the temperature averaged rate coefficient  $L_3$  from the two-body resonance model employed in [16] and from our three-body calculation are very similar, the energy-dependent recombination rate  $K_3(E)$  shows significant differences. New experiments at lower temperatures  $T \leq 0.5 \mu\text{K}$  should be able to distinguish between the two scenarios and determine the nature of the microscopic physics responsible for the loss processes.

In summary, we have shown that the three-body recombination rate coefficient  $K_3(E)$  for spin-polarized  ${}^6\text{Li}$  atoms with resonant  $p$ -wave interactions possesses interesting features due to two- and three-body resonances which can be seen at low temperatures. We also have demonstrated that three-body loss data can be used to extract detailed information on the two-body interaction once a reliable parameterization is established and used in a full three-body calculation. Our effective field theory approach has the additional advantage that the interaction is directly given in terms of the effective range parameters.

Waseem *et al.* recently described the unitary regime using a model for cascade processes that leads to a modified three-body loss coefficient  $L_3$  [17]. Our uncertainty analysis led us to exclude this regime as more partial wave channels are expected to contribute to the loss rate at these temperatures. It would therefore be interesting to include additional partial wave channels in our calculation of the total loss rate in order to test their result and to analyze whether it is really necessary to include additional recombination mechanisms to achieve agreement with the data.

We finally note that the S-wave scattering between the  $|F = 1/2, m_F = +1/2\rangle$  and  $|F = 1/2, m_F = -1/2\rangle$  hyperfine states of  ${}^6\text{Li}$  is moderately large (and negative) at the magnetic fields considered in this work [34]. The study of recombination losses in this two-component system of identical fermions with large  $s$ - and  $p$ -wave scattering lengths might

therefore lead to interesting features such as a competition between odd and even parity recombination channels.

### Acknowledgments

M.S. thanks the nuclear theory groups of UT Knoxville and Oak Ridge National Laboratory for their kind hospitality during his research stay. H.W.H and L.P. thank the Institute for Nuclear Theory at the University of Washington for its kind hospitality and stimulating research environment. L.P. thanks the nuclear theory group of TU Darmstadt for its hospitality during the final stages of this work. This research was supported by the Deutsche Forschungsgemeinschaft (DFG, German Research Foundation) – Projektnummer 279384907 – SFB 1245, by the National Science Foundation under Grant No. PHY-1555030, by the Office of Nuclear Physics, U.S. Department of Energy under contracts No. DE-AC05-00OR22725 and No. DE-FG02-00ER41132.

### Appendix A: Lagrangian

The EFT Lagrangian for the spin-polarized fermions can be split into three parts:  $\mathcal{L} = \mathcal{L}_1 + \mathcal{L}_2 + \mathcal{L}_3$ . For  ${}^6\text{Li}$  atoms with mass  $m = 6.0151223(5)$  u [35], the one-body part

$$\mathcal{L}_1 = \psi^\dagger \left[ i\partial_0 + \frac{\nabla^2}{2m} \right] \psi \quad (\text{A1})$$

can be written in terms of scalar fields  $\psi, \psi^\dagger$  which anticommute.

The remaining parts comprise all two- and three-body contact terms compliant with Galilean symmetry. They are formulated using bosonic fields  $\pi_{m_l}, \pi_{m_l}^\dagger$  ( $m_l \in \{-1, 0, 1\}$ ), which annihilate and create two atoms in a  $p$ -wave, respectively. At LO,  $\mathcal{L}_2$  reads

$$\begin{aligned} \mathcal{L}_2 = & \pi_{m_l}^\dagger \left[ \Delta + \left( i\partial_0 + \frac{\nabla^2}{4m} \right) + \dots \right] \pi_{m_l} \\ & - \frac{g}{\sqrt{2}} \left[ \pi_{m_l}^\dagger \left( \psi \left\{ -i\overleftrightarrow{\nabla}_2 \right\}_{1m_l} \psi \right) + \text{H.c.} \right], \end{aligned} \quad (\text{A2})$$

where ‘‘H.c.’’ is the Hermitian conjugate and the sums over  $m_l$  are implicit. The  $p$ -wave nature of the diatom manifests itself in the tensor structure  $\{\cdot\}_{1m_l}$ . Together with the Galilean-invariant derivative  $\overleftrightarrow{\nabla}_2 \equiv (\overleftarrow{\nabla} - \overrightarrow{\nabla})/2$ , it contributes a factor

$$\{\mathbf{k}\}_{1m_l} \equiv (4\pi/3)^{1/2} k Y_1^{m_l}(\hat{\mathbf{k}}) \quad (\text{A3})$$

to the  $\pi$ - $\psi\psi$  vertex. Here,  $\mathbf{k} = (\mathbf{k}_1 - \mathbf{k}_2)/2$  is the atom-atom relative momentum. To describe a shallow  $p$ -wave resonance, two real low-energy parameters are required [26, 36]. They are chosen as  $\Delta$  and the coupling  $g$  which both will be matched to observables.

The three-body part  $\mathcal{L}_3$  contains three-body interactions which eliminate potential divergences in different spin-parity channels  $J^P$ . At LO, a single three-body force ( $J^P = 1^+$ ) enters the theory. It takes the form

$$\mathcal{L}_3 = -C_0^{(1+)} \frac{12\pi}{mg^2} (\psi \boldsymbol{\pi})_{m_J}^{(1+)\dagger} (\psi \boldsymbol{\pi})_{m_J}^{(1+)} + \dots \quad (\text{A4})$$

with the  $J^P = 1^+$  ( $l = L = J = 1$ ) field combinations

$$(\psi \boldsymbol{\pi})_{m_J}^{(1^+)} = \sqrt{3} C_{1m_L, 1m_i}^{1m_J} \psi \left\{ -i \overleftrightarrow{\nabla}_3 \right\}_{1m_L} \pi_{m_i} \quad (\text{A5})$$

and the Galileian-invariant derivative  $\overleftrightarrow{\nabla}_3 \equiv (2\overleftarrow{\nabla} - \overrightarrow{\nabla})/3$ . Further, we define dimensionless three-body force  $H^{(1^+)}$  with

$$C_0^{(1^+)}(\Lambda) = H^{(1^+)}(\Lambda)/\Lambda^2. \quad (\text{A6})$$

## Appendix B: Faddeev equation

The Feynman rules resulting from the Lagrangian given in the previous section can be used to derive an integral equation for atom-dimer scattering. For orbital angular momentum quantum numbers  $l = l' = 1$  and projection  $m_l$  and  $m_{l'}$ , respectively, this integral equation is given by

$$\begin{aligned} T^{m_l, m_{l'}}(\mathbf{p}, \mathbf{p}'; p_E) &= -V^{m_l, m_{l'}}(\mathbf{p}, \mathbf{p}'; p_E) \\ &+ \sum_{m_{l''}} \int \frac{d^3q}{(2\pi)^3} V^{m_l, m_{l''}}(\mathbf{p}, \mathbf{q}; p_E) G_\pi(\tilde{k}(q^2)) T^{m_{l''}, m_{l'}}(\mathbf{q}, \mathbf{p}'; p_E), \end{aligned} \quad (\text{B1})$$

where  $\tilde{k}(q^2)$  is given in Eq. (9). The particle exchange potential is given by

$$-iV^{m_l, m_{l'}}(\mathbf{p}, \mathbf{q}; p_E) = -i24\pi \frac{\{\mathbf{q} + \mathbf{p}/2\}_{1m_l}^* \{\mathbf{p} + \mathbf{q}/2\}_{1m_{l'}}}{p^2 + q^2 - p_E^2 + \mathbf{p} \cdot \mathbf{q}} \quad (\text{B2a})$$

$$\begin{aligned} &= -i \sum_J \sum_{L, L'} V^{3L_J, 3L'_J}(p, q; p_E) \\ &\times 4\pi \sum_{m_J} (\mathbf{Y}_{(L,1)Jm_J}(\hat{\mathbf{p}}))^{m_l} (\mathbf{Y}_{(L',1)Jm_J}(\hat{\mathbf{q}}))^{m_{l'}}^*. \end{aligned} \quad (\text{B2b})$$

Projection onto partial waves with  $l = 1$ , total orbital angular momentum  $L$ , and total angular momentum  $J$  yields

$$\begin{aligned} V^{3L_J, 3L'_J}(p, q; p_E) &= -24\pi \frac{\sqrt{(2L+1)(2L'+1)}}{2J+1} \\ &\times \left[ C_{L0,10}^{J0} C_{L'0,10}^{J0} \frac{1}{2} \left( \frac{p}{q} \hat{t}_{L'} + \frac{q}{p} \hat{t}_L \right) \right. \\ &\quad \left. + pq \left( \frac{1}{4} C_{L0,10}^{J0} C_{L'0,10}^{J0} \hat{t}_J + (2J+1) \sum_k C_{L0,10}^{k0} C_{L'0,10}^{k0} \begin{Bmatrix} 1 & J & L' \\ 1 & k & L \end{Bmatrix} \hat{t}_k \right) \right] \\ &\times Q. \left( \frac{p_E^2 - p^2 - q^2}{pq} \right) \end{aligned} \quad (\text{B3})$$

where  $Q.$  are Legendre functions of the second kind in the convention of Ref. [32] and the short notation  $\hat{t}_L Q. \equiv Q_L$  was used. For the  $1^+$  channel ( $l = L = J = 1$ ), we recover Eq. (11).

---

[1] E. Braaten and H.-W. Hammer, Phys. Rept. **428**, 259 (2006), cond-mat/0410417.

- [2] S. Giorgini, L. P. Pitaevskii, and S. Stringari, *Rev. Mod. Phys.* **80**, 1215 (2008).
- [3] C. Chin, R. Grimm, P. Julienne, and E. Tiesinga, *Rev. Mod. Phys.* **82**, 1225 (2010).
- [4] P. Naidon and S. Endo, *Rept. Prog. Phys.* **80**, 056001 (2017), 1610.09805.
- [5] C. H. Greene, P. Giannakeas, and J. Pérez-Ríos, *Rev. Mod. Phys.* **89**, 035006 (2017).
- [6] V. Efimov, *Phys. Lett.* **33B**, 563 (1970).
- [7] E. Nielsen and J. H. Macek, *Phys. Rev. Lett.* **83**, 1566 (1999).
- [8] B. D. Esry, C. H. Greene, and J. P. Burke, *Phys. Rev. Lett.* **83**, 1751 (1999).
- [9] P. F. Bedaque, E. Braaten, and H.-W. Hammer, *Phys. Rev. Lett.* **85**, 908 (2000), cond-mat/0002365.
- [10] E. Braaten and H.-W. Hammer, *Phys. Rev. Lett.* **87**, 160407 (2001), cond-mat/0103331.
- [11] T. Kraemer, M. Mark, P. Waldburger, J. G. Danzl, C. Chin, B. Engeser, A. D. Lange, K. Pilch, A. Jaakkola, H.-C. Naegerl, et al., *Nature* **440**, 315 (2006).
- [12] J. Zhang et al., *Phys. Rev. A* **70**, 030702 (2004).
- [13] C. H. Schunck, M. W. Zwierlein, C. A. Stan, S. M. F. Raupach, W. Ketterle, A. Simoni, E. Tiesinga, C. J. Williams, and P. S. Julienne, *Phys. Rev. A* **71**, 045601 (2005).
- [14] C. A. Regal, C. Ticknor, J. L. Bohn, and D. S. Jin, *Phys. Rev. Lett.* **90**, 053201 (2003).
- [15] J. Yoshida, T. Saito, M. Waseem, K. Hattori, and T. Mukaiyama, *Phys. Rev. Lett.* **120**, 133401 (2018).
- [16] M. Waseem, J. Yoshida, T. Saito, and T. Mukaiyama, *Phys. Rev. A* **98**, 020702 (2018).
- [17] M. Waseem, J. Yoshida, T. Saito, and T. Mukaiyama, *Phys. Rev. A* **99**, 052704 (2019).
- [18] M. Jona-Lasinio, L. Pricoupenko, and Y. Castin, *Phys. Rev. A* **77**, 043611 (2008), 0708.0610.
- [19] Y. Nishida, *Phys. Rev.* **A86**, 012710 (2012), 1111.6961.
- [20] E. Braaten, P. Hagen, H.-W. Hammer, and L. Platter, *Phys. Rev. A* **86**, 012711 (2012), 1110.6829.
- [21] H.-W. Hammer and L. Platter, *Ann. Rev. Nucl. Part. Sci.* **60**, 207 (2010), 1001.1981.
- [22] H. W. Hammer, S. König, and U. van Kolck (2019), 1906.12122.
- [23] T. Nakasuji, J. Yoshida, and T. Mukaiyama, *Phys. Rev. A* **88**, 012710 (2013).
- [24] J. Levinsen, N. R. Cooper, and V. Gurarie, *Phys. Rev. A* **78**, 063616 (2008).
- [25] G. M. Bruun, A. D. Jackson, and E. E. Kolomeitsev, *Phys. Rev. A* **71**, 052713 (2005).
- [26] P. F. Bedaque, H.-W. Hammer, and U. van Kolck, *Phys. Lett. B* **569**, 159 (2003), nucl-th/0304007.
- [27] M. Schmidt, Ph.D. thesis, Technische Universität, Darmstadt (2019), URL <http://tuprints.ulb.tu-darmstadt.de/8778/>.
- [28] E. Braaten and H. W. Hammer, *Phys. Rev.* **A70**, 042706 (2004), cond-mat/0303249.
- [29] B. D. Esry, C. H. Greene, and H. Suno, *Phys. Rev. A* **65**, 010705 (2001).
- [30] H. Suno, B. D. Esry, and C. H. Greene, *Phys. Rev. Lett.* **90**, 053202 (2003).
- [31] J. P. D’Incao, H. Suno, and B. D. Esry, *Phys. Rev. Lett.* **93**, 123201 (2004).
- [32] M. Abramowitz and I. A. Stegun, *Handbook of Mathematical Functions* (Dover, New York, 1964).
- [33] H. Suno, B. D. Esry, and C. H. Greene, *New J. Phys.* **5**, 53 (2003).
- [34] P. S. Julienne and J. M. Hutson, *Phys. Rev. A* **89**, 052715 (2014).
- [35] J. R. de Laeter *et al.*, *Pure Appl. Chem.* **75**, 683 (2003).
- [36] C. A. Bertulani, H.-W. Hammer, and U. Van Kolck, *Nucl. Phys. A* **712**, 37 (2002), nucl-th/0205063.